Gravitationally redshifted absorption lines in the X-ray burst spectra of a neutron star

J. Cottam*, F. Paerels† & M. Mendez‡

** NASA Goddard Space Flight Center, Laboratory for High Energy Astrophysics, Greenbelt, Maryland 20771, USA*
† Columbia Astrophysics Laboratory and Department of Astronomy, Columbia University, 538 West 120th Street, New York, New York 10027, USA
‡ SRON National Institute for Space Research, Sorbonnelaan 2, 3584 CA Utrecht, The Netherlands

The fundamental properties of neutron stars provide a direct test of the equation of state of cold nuclear matter, a relationship between pressure and density that is determined by the physics of the strong interactions between the particles that constitute the star. The most straightforward method of determining these properties is by measuring the gravitational redshift of spectral lines produced in the neutron star photosphere[1]. The equation of state implies a mass–radius relation, while a measurement of the gravitational redshift at the surface of a neutron star provides a direct constraint on the mass-to-radius ratio. Here we report the discovery of significant absorption lines in the spectra of 28 bursts of the low-mass X-ray binary EXO0748−676. We identify the most significant features with the Fe XXVI and XXV $n = 2$–3 and O VIII $n = 1$–2 transitions, all with a redshift of $z = 0.35$, identical within small uncertainties for the respective transitions. For an astrophysically plausible range of masses ($M \approx 1.3$–2.0 solar masses; refs 2–5), this value is completely consistent with models of neutron stars composed of normal nuclear matter, while it excludes some models[6,7] in which the neutron stars are made of more exotic matter.

The XMM-Newton observatory[8] observed the low-mass X-ray binary EXO0748−676 (ref. 9) during its commissioning and calibration phases for almost a half million seconds, spread over six satellite orbits between 21 February 2000 and 21 April 2000. Data were recorded with the Reflection Grating Spectrometer[10] (RGS) for 335,000 s (data obtained with the European Photon Imaging Cameras[11,12] (EPIC) are available for 39,000 s of simultaneous exposure). During this time, a total of 28 X-ray bursts were recorded with the RGS, lasting a cumulative 3,200 s. During the brief bursts, the neutron star outshines the accretion-generated light by an order of magnitude in intensity, while the continuing accretion ensures a continuing supply of heavy elements in the stellar photosphere. This makes the burst spectrum a promising place to detect absorption structure from a neutron star photosphere, a long-standing goal in compact-object astrophysics. With a detailed stellar photospheric spectrum, the techniques of classical stellar spectroscopy could be used to measure the fundamental parameters of neutron stars. It should also be possible to measure the general relativistic gravitational redshift, which provides additional constraints on the mass and radius of the star. Owing to the long exposure, and the high efficiency and spectral resolving power of the RGS, this EXO0748−676 dataset is by far the most sensitive to date for conducting such a search.

Data were processed with the XMM-Newton Science Analysis Software (SAS) that is currently available as version 5.3.3. The soft-X-ray light curve of EXO0748−676 shows considerable variability[13]. Searching for X-ray bursts in the RGS light curve, we considered only events which conformed to the step rise/exponential decay shape characteristic of type I X-ray bursts[14]. We identified 28 bursts in the RGS data. The bursts varied in peak intensity between 4 counts s^{-1} and 12 counts s^{-1} with an average of 8.8 counts s^{-1}. This represents an increase by a factor of ~15 over the quiescent levels observed in the periods of low activity. We defined the onset of a burst as the time at which the count rate first rises above the quiescent level by a factor of two or more. The end, less well defined, occurs when the count rate drops back to the local average level. Most bursts ranged in duration from 48 to 128 s, with an average of 90 s. Seven of the bursts were longer, with durations between 176 and 320 s.

We then extracted the first-order RGS spectra for each burst. The spacecraft pointing was stable during observations on each of the separate revolutions, but differed between revolutions by up to 40 arcsec. To generate the average burst spectrum we therefore combined the data for all observations within a single revolution, but generated separate spectral files and response matrices for each revolution. All spectral fitting was performed simultaneously on these separate data sets. For ease of display we generated a flux spectrum of the average burst, using the effective area curves for each separate data set. This allowed us to combine the data from the two RGS instruments as well. The wavelength scale is accurate to ~10 mÅ. The effective area is accurate to 5% for all wavelengths longer than 8 Å (ref. 10). Background subtraction was performed using the same extraction algorithms, but over the image region not occupied by the source. The background flux is a significant fraction of the total flux for wavelengths longer than ~32 Å. We therefore considered only the wavelength range from 8 to 32 Å in our analysis.

To constrain the broadband properties of the burst spectrum we examined the EPIC data. Pile-up during the bright bursts contaminated all but 250 s, or three bursts. The EPIC pn-CCD spectrum of these three bursts is well fitted by a black body, with a peak colour temperature of $kT_{BB} \approx 1.8$ keV, decaying to $kT_{BB} \leq 1.5$ keV. As the spectral properties clearly evolve during the bursts, we investigated the RGS spectrum of the early, bright phases and the decay phases separately. We explored a variety of ways to subdivide the bursts, but found that the results were not sensitive to the exact criterion used to compile the 'early'- and 'late'-time burst spectra. We therefore chose to divide the bursts in the simplest way, by splitting them in half by duration. The resulting flux spectra for the early and late phases of the averaged burst are shown in Fig. 1.

As in the case of the quiescent spectrum[13], there is clear evidence for absorption and emission from highly ionized gas surrounding the neutron star during the bursts. O VII K-shell emission (consisting of $n = 1$–2 resonance, intercombination and forbidden lines at 21.60, 21.80 and 22.10 Å) are clearly detected, as is absorption by O VII (photoelectric absorption at 16.78 Å, resonance line absorption at 21.60 Å). The fact that the O VII line emission is dominated by the intercombination transition indicates that the gas is recombining, which implies that the ionization is driven by photoionization, and that the electron density is relatively high ($n_e \geq 10^{12}$ cm^{-3}). We saw a clear change in the nature of the O VII spectrum as the bursts progressed, with the emission weakening and the absorption increasing from the early to the late phases, indicative of an overall progressive flattening of the source geometry towards the line of sight. Wavelength shifts in the O VII absorption features indicate a significant bulk outflow velocity of $v \approx 5{,}000$ km s^{-1} during the bursts.

In order to develop a physically consistent model for the spectral transmission of the circumstellar absorber, which we need in order to quantitatively account for its contribution to the observed absorption spectra, we fitted the O VII and O VIII spectra and measured the intensity, velocity width and Doppler shifts of the emission lines, and the ion-column density and velocity broadening of the absorption features for both the early- and late-phase spectra. The model assumes an empirical continuum spectrum during the bursts, constructed from a black body and a power law, whose parameters were optimized by eye. O VII and O VIII absorption spectra were calculated with a spectral code originally developed to interpret the X-ray absorption spectra of active galactic nuclei

(AGN)[15]. The model incorporates atomic structure and transition probabilities, and, for any given ion, consistently accounts for the absorption in all transitions out to high principal quantum number and the photoelectric continuum. The entire spectrum is subject to absorption by a neutral medium, with equivalent hydrogen-column density $N_H = 1 \times 10^{21}$ cm^{-2}; the neutral absorption spectrum has strong O K absorption in the 22–24 Å range, the shape of which we optimized to conform to the interstellar O absorption spectrum measured in other sources[16].

We then synthesized a model for the full spectral transmission of the circumstellar absorber. We adopted an ionization parameter, $\xi \equiv L_{ionizing}/n_e R^2$ (with $L_{ionizing}$ the ionizing luminosity, n_e the electron density of the medium, R its distance to the ionizing source[17,18]), of $\xi = 10$ as representative, so as not to overproduce O VIII absorption, and added the other elements at their solar abundances, with ionization fractions derived from the photoionization equilibrium balance. The full set of ions included the K-shell ions of C, N, O, Ne, Mg and Si, and the L-shell ions of Fe. We scaled the turbulent velocity broadening of each ion with the value measured in the O VII resonance line, assuming a common temperature for all ions. We adopted the Doppler blueshift observed in the O VII features for all ions. The resulting transmission model, superimposed on the optimized continuum model, is overplotted on the observed spectra in Fig. 1. The apparent absence of the N VII Lyman α (Lyα) absorption at λ 24.78 Å in the data implies a subsolar N/O ratio in the absorbing gas. The absence, in the data, of absorption by ions that are present at higher ionization parameter—specifically the absence of significant Fe L absorption—implies that the circumstellar medium occupies only a narrow range of (fairly low) ionization parameters.

We then examined the spectrum for any remaining structure that is not associated with the circumstellar absorber. In the early-time burst spectrum, the most significant modulation appears at 13.0 Å. We also see weaker structure at 25.3, 26.3 and 26.9 Å. In the late-time spectrum, we identify significant modulations at 13.75, 25.2 and 26.4 Å with weak features at 17.8 and 19.7 Å. In view of the noise levels, it is difficult to perform such a search effectively using statistical significance criteria only. We will therefore appeal to spectroscopic consistency arguments when assessing apparent absorption features in the spectrum. As a guide, however, we estimated the significance of the features by fitting each with a simple gaussian profile, optimizing the continuum, and evaluating their significance in terms of the amplitude of the gaussian. In the early-phase spectrum, the depth of the 13.0 Å feature differs by 7 σ from zero, whereas those of the 25.3, 26.3 and 26.9 Å features differ by 3–4 σ. In the late-phase spectrum, the 13.75 Å feature has a 5 σ amplitude, and the 25.2 and 26.4 Å features each have amplitudes of 3 σ. The features at 17.8 and 19.7 Å in the late-phase spectrum have amplitudes less than 1 σ, and we therefore exclude these features from further consideration.

We inspected the spectra obtained by the two RGS spectrometers separately and found that all the features appear in both parallel spectra, but with only marginal detections in the case of the 25.3, 26.3 and 26.9 Å (early-times) features. The fact that all significant features appear either at early or at late times rules out the possibility of stationary modulations in the spectrometer efficiency. We have also examined the three very deep RGS spectra of extragalactic featureless continuum sources (Mkn421, 3C273 and PKS2155−304; A. P. Rasmussen *et al.*, manuscript in preparation). No significant modulations were observed in these spectra at the positions of the features under discussion, nor did these spectra exhibit unexplained features at any other wavelength, of strength comparable to those observed here.

Neither do the features match the wavelengths of absorption lines

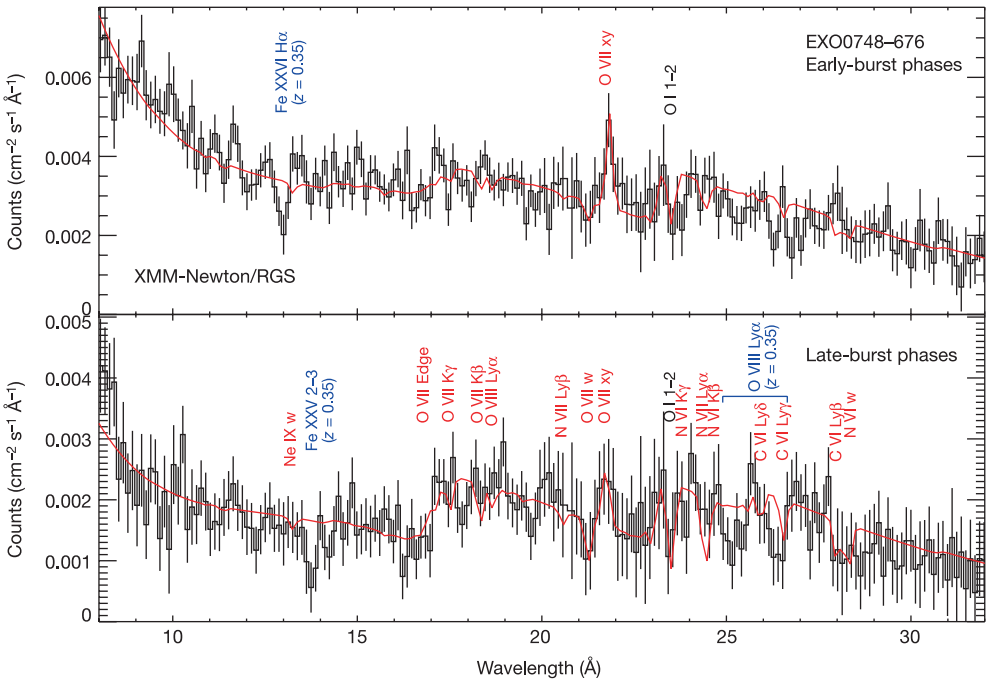

Figure 1 The XMM-Newton RGS spectra of EXO0748−676 for 28 type I X-ray bursts. The background-subtracted flux spectra for the early and late phases of the bursts are shown in the top and bottom panels, respectively. The data are plotted as the black histograms, with 1 σ error bars derived from counting statistics. The red line is the empirical continuum, with additional O VII intercombination line emission, modulated by absorption in photoionized circumstellar material. Red labels show the positions of the most prominent discrete absorption lines from the circumstellar medium; in the He-like spectra, 'w' signifies the $n = 1$–2 resonance transition, 'xy' the (unresolved) $n = 1$–2 intercombination transitions, while higher series members are marked 'Kβ,γ', and so on. Column densities in ions other than O VII have been normalized to the absorption measured in O VII, assuming an ionization parameter $\xi = 10$, and solar abundances. The N VII Lyα line at 24.78 Å is overpredicted, indicating a subsolar N/O abundance ratio. Black labels indicate the interstellar O 1*s*–2*p* absorption line. Blue labels indicate the photospheric absorption lines in Fe XXVI, Fe XXV and O VIII, at a redshift $z = 0.35$. The data and models have been rebinned to $\Delta\lambda = 0.124$ Å, which is about 2.5 times larger than the RGS instrument resolution.

expected from the circumstellar absorber, with the possible exception of the 26.4 Å feature in the late-phase spectrum, which is probably partly due to C VI Lyman γ (Lyγ) at 26.6 Å. We examined absorption models appropriate to higher ionization parameters (over the range $\xi = 10$–100) and found that the features cannot be made consistent with circumstellar absorption at any ionization parameter. This explanation can be rejected on purely spectroscopic grounds: it requires significant velocity shifts that vary randomly between ions that are present at similar ionization parameters. Furthermore, fitting individual absorption lines to the features produced serious inconsistencies in terms of the predicted overall absorption structure due to any given single ion. Finally, the features do not appear in the (accretion-dominated) quiescent spectrum of the source.

We are left with the possibility that the absorption features arise in the photosphere of the neutron star. The magnetic fields in the neutron stars in low-mass X-ray binaries are believed to be small[19–21], so that field effects do not affect the atomic structure, and we can use well-established atomic spectroscopy to interpret the wavelengths. In the only other example of non-trivial structure in the spectrum of a neutron star[22], the correct spectroscopic identification, and hence the inferred redshift, depends critically on the unknown strength of the stellar magnetic field. We note that the previous detections of large equivalent-width features in the 4–5 keV band with proportional counters[23] have not been substantiated by subsequent observations[24], and that these and other similar detections[25,26] are most probably due to instrumental effects.

We have examined all the spectra of the K-shell ions of C through to and including Si, and find no multiple coincidences between observed and predicted line positions, with identical redshifts for all ions. However, an important clue to identifying the features lies in the presence of the 13.0 Å line at early times and the presence of the 13.75 Å line at late times. A solution to the Saha ionization balance for densities $n \approx 10^{23}\,\mathrm{cm}^{-3}$ (as expected in a neutron star atmosphere at a Rosseland optical depth of unity, above which most of the absorption spectrum is formed) indicates that iron should be primarily in its H-like charge state at temperatures $kT \geq 1.2$ keV, whereas at $kT \leq 1.2$ keV, the He-like charge state dominates; these temperatures roughly correspond to the observed colour temperature early and late in the bursts, respectively. At these temperatures, the ionization balance of iron does not shift into the fully stripped charge state until the density drops below $\sim 10^{22}\,\mathrm{cm}^{-3}$. The density and temperature in a real atmosphere exhibit significant gradients, but the Saha balance at a representative temperature and density usually provides a good indication as to which ions of a given element are likely to be dominant in the stellar absorption spectrum. The $n = 2$–3 transitions in the H-like ion (the analogue of the Hα Balmer line) occur at 9.518, 9.533, 9.579 and 9.675, 9.690, 9.738 Å (ref. 27). Identifying these transitions with the feature at 13.0 Å in the early-phase burst spectrum implies a redshift of $z = 0.35$. The strongest $n = 2$–3 transitions in the He-like ion occur at 10.213, 10.048 Å (E. Behar, personal communication; the 10.213 Å transition has the highest oscillator strength). Identifying these transitions with the feature at 13.75 Å in the late-phase spectrum also implies a redshift of $z = 0.35$. Members of higher-order series will all lie at wavelengths lower than 10 Å, to which our spectrum is not sensitive.

The Saha balance at temperatures $kT \geq 1$ keV and densities $n \approx 10^{23}\,\mathrm{cm}^{-3}$ indicates that all the lighter elements should be nearly stripped, so we would not expect to see their K-shell absorption lines, with the possible exception of oxygen, in view of its relatively high abundance. Applying the same redshift to the O VIII Lyα line (rest wavelength 18.97 Å) we would expect to see a feature at 25.6 Å. We speculate that the double (wavelengths 25.2 and 26.4 Å) structure observed at late phases, which is centred at this wavelength, is in fact a self-reversed, broad O VIII Lyα line, where the self-reversed profile is indicative of extended structure to the outer atmosphere, and possibly a slow outflow, such as observed in the strong ultraviolet resonance lines in massive stars with extended atmospheres[28]. The corresponding O VIII Lyman β (Lyβ) line (21.60 Å at $z = 0.35$) would be hidden in the O VII spectrum from the circumstellar medium. The remaining features are all of relatively low significance, have no obvious spectroscopic interpretation, and are probably statistical fluctuations. A quantitative interpretation of the strength and shape of the features we have identified will have to await a dedicated full model-atmosphere calculation, which may have to incorporate effects induced by the X-ray bursts.

We have identified three sets of redshifted transitions in iron and oxygen in the EXO0748−676 spectrum, all with an implied redshift of $z = 0.35$. We have compared our result with the family of theoretical mass–radius relations in ref. 6. A redshift of $z = 0.35$ is consistent with most modern equations of state for neutron stars composed of normal matter in the mass range of $M \approx 1.4$–1.8 solar masses and in the radius range of $R \approx 9$–12 km, depending on the choice of M–R relation. This is compatible with a neutron star with a birth mass near the average for non-accreting neutron stars ($M = 1.4$ solar masses), that has been accreting mass at the observed rate for $\sim 10^9$ years, and agrees with the estimated masses of other accreting neutron stars[2–4]. A redshift of $z = 0.35$ is inconsistent with several M–R relations based on equations of state for more exotic matter such as strange quark matter or kaon condensates[6,7], unless, for some of these equations of state, the mass of the neutron star in EXO0748−676 is ≤ 1.1 solar masses, which is lower than predicted by astrophysical arguments. □

Received 4 July; accepted 24 September 2002; doi:10.1038/nature01159.

1. van Paradijs, J. Possible observational constraints on the mass-radius relation of neutron stars. *Astrophys. J.* **234,** 609–611 (1979).
2. Thorsett, S. E. & Chakrabarty, D. Neutron star mass measurements. I. Radio pulsars. *Astrophys. J.* **512,** 288–299 (1999).
3. Barziv, O., Kaper, L., Van Kerkwijk, M. H., Telting, J. H. & Van Paradijs, J. The mass of the neutron star in Vela X-1. *Astron. Astrophys.* **377,** 925–944 (2001).
4. Orosz, J. A. & Kuulkers, E. The optical light curves of Cygnus X-2 (V1341 Cyg) and the mass of its neutron star. *Mon. Not. R. Astron. Soc.* **305,** 132–142 (1999).
5. Zhang, W., Smale, A. P., Strohmayer, T. E. & Swank, J. H. Correlation between energy spectral states and fast time variability and further evidence for the marginally stable orbit in 4U 1820−30. *Astrophys. J.* **500,** L171–L174 (1998).
6. Lattimer, J. M. & Prakash, M. Neutron star structure and the equation of state. *Astrophys. J.* **550,** 426–442 (2001).
7. Dey, M., Bombaci, I., Dey, J., Ray, S. & Samanta, B. C. Strange stars with realistic quark vector interaction and phenomenological density-dependent scalar potential. *Phys. Lett. B* **438,** 123–128 (1998) ; erratum **467,** 303–305 (1999).
8. Jansen, F. *et al.* The XMM-Newton observatory. I. The spacecraft and operations. *Astron. Astrophys.* **365,** L1–L6 (2001).
9. Parmar, A. N., White, N. E., Giommi, P. & Gottwald, M. The discovery of 3.8 hour periodic intensity dips and eclipses from the transient low-mass X-ray binary EXO 0748−676. *Astrophys. J.* **308,** 199–212 (1986).
10. den Herder, J. W. *et al.* The Reflection Grating Spectrometer on board XMM-Newton. *Astron. Astrophys.* **365,** L7–L17 (2001).
11. Turner, M. J. L. *et al.* The European Photon Imaging Camera on XMM-Newton: The MOS cameras. *Astron. Astrophys.* **365,** L27–L35 (2001).
12. Strüder, L. *et al.* The European Photon Imaging Camera on XMM-Newton: The pn-CCD camera. *Astron. Astrophys.* **365,** L18–L26 (2001).
13. Cottam, J., Kahn, S. M., Brinkman, A. C., den Herder, J. W. & Erd, C. High-resolution spectroscopy of the low-mass X-ray binary EXO 0748−67. *Astron. Astrophys.* **365,** L277–L281 (2001).
14. Lewin, W. H. G., van Paradijs, J. & Taam, R. E. X-Ray bursts. *Space Sci. Rev.* **62,** 223 (1993).
15. Sako, M. *et al.* Complex resonance absorption structure in the X-ray spectrum of IRAS 13349+2438. *Astron. Astrophys.* **365,** L168–L173 (2001).
16. Paerels, F. *et al.* Interstellar X-ray absorption spectroscopy of oxygen, neon, and iron with the CHANDRA LETGS spectrum of X0614+091. *Astrophys. J.* **546,** 338–344 (2001).
17. Tarter, C. B., Tucker, W. H. & Salpeter, E. E. The interaction of X-ray sources with optically thin environments. *Astrophys. J.* **156,** 943–952 (1969).
18. Kallman, T. R. & McCray, R. X-ray nebular models. *Astrophys. J. Suppl. Ser.* **50,** 263–317 (1982).
19. Wijnands, R. & van der Klis, M. A millisecond pulsar in an X-ray binary system. *Nature* **394,** 344–346 (1998).
20. Galloway, D. K., Chakrabarty, D., Morgan, E. H. & Remillard, R. A. Discovery of a high-latitude accreting millisecond pulsar in an ultracompact binary. *Astrophys. J.* **576,** L137–L140 (2002).
21. Psaltis, D. & Chakrabarty, D. The disk-magnetosphere interaction in the accretion-powered millisecond pulsar SAX J1808.4-3658. *Astrophys. J.* **521,** 332–340 (1999).
22. Sanwal, D., Pavlov, G. G., Zavlin, V. E. & Teter, M. A. Discovery of absorption features in the X-ray spectrum of an isolated neutron star. *Astrophys. J.* **574,** L61–L64 (2002).
23. Waki, I. *et al.* Discovery of absorption lines in X-ray burst spectra from X1636-536. *Publ. Astron. Soc. Jpn* **36,** 819–830 (1984).

24. Sztajno, M. *et al.* Unusual X-ray burst profiles from 4U/MXB 1636-53. *Astrophys. J.* **299,** 487–495 (1985).
25. Nakamura, N., Inoue, H. & Tanaka, Y. Detection of absorption lines in the spectra of X-ray bursts from X1068-52. *Publ. Astron. Soc. Jpn* **40,** 209–217 (1988).
26. Magnier, E. *et al.* A 4.1 keV spectral feature in a type 1 X-ray burst from EXO 1747-214. *Mon. Not. R. Astron. Soc.* **237,** 729–738 (1989).
27. Bethe, H. A. & Salpeter, E. E. *Quantum Mechanics of One and Two Electron Atoms* (Plenum, New York, 1977).
28. Kudritzki, R. P. & Hummer, D. G. Quantitative spectroscopy of hot stars. *Annu. Rev. Astron. Astrophys.* **28,** 303–345 (1990).

Acknowledgements This work is based on observations obtained with the XMM-Newton, an ESA science mission with instruments and contributions directly funded by ESA member states and the USA (NASA). We thank E. Behar for supplying us with results from his atomic-structure calculations of the He-like Fe ion, and M. Sako for the use of his absorption spectral code.

Competing interests statement The authors declare that they have no competing financial interests.

Correspondence and requests for materials should be addressed to J.C. (e-mail: jcottam@milkyway.gsfc.nasa.gov).

Pressure-induced crystallization of a spin liquid

I. Mirebeau*, I. N. Goncharenko*, P. Cadavez-Peres*, S. T. Bramwell†, M. J. P. Gingras‡§ & J. S. Gardner‖

** Laboratoire Léon Brillouin, CEA-CNRS, CE Saclay, 91191 Gif sur Yvette, France*
† Department of Chemistry, University College London, 20 Gordon Street, London WC1H OAJ, UK
‡ Department of Physics, University of Waterloo, Waterloo, Ontario N2L 3G1, Canada
§ Canadian Institute for Advanced Research, 180 Dundas Street, Toronto, Ontario M5G 1Z8, Canada
‖ Neutron Program for Materials Research, National Research Council of Canada, Chalk River, Ontario KOJ 1J0, Canada

Liquids are expected to crystallize at low temperature. The only exception is helium, which can remain liquid at 0 K, owing to quantum fluctuations[1,2]. Similarly, the atomic magnetic moments (spins) in a magnet are expected to order at a temperature scale set by the Curie–Weiss temperature θ_{CW} (ref. 3). Geometrically frustrated magnets represent an exception. In these systems, the pairwise spin interactions cannot be simultaneously minimized because of the lattice symmetry[4]. This can stabilize a liquid-like state of short-range-ordered fluctuating moments well below θ_{CW} (refs 5–7). Here we use neutron scattering to observe the spin liquid state in a geometrically frustrated system, $Tb_2Ti_2O_7$, under conditions of high pressure (~9 GPa) and low temperature (~ 1 K). This compound is a three-dimensional magnet with $\theta_{CW} = -19$ K, where the negative value indicates antiferromagnetic interactions. At ambient pressure $Tb_2Ti_2O_7$ remains in a spin liquid state down to at least 70 mK (ref. 8). But we find that, under high pressure, the spins start to order or 'crystallize' below 2.1 K, with antiferromagnetic order coexisting with liquid-like fluctuations. These results indicate that a spin liquid/solid mixture can be induced by pressure in geometrically frustrated systems.

$Tb_2Ti_2O_7$ is an insulating pyrochlore oxide in which localized Tb^{3+} spins occupy a lattice of corner-linked tetrahedra. Antiferromagnetic Heisenberg interactions on this lattice are highly frustrated, giving rise to macroscopic degeneracy in the ground state[4]. The pyrochlore lattice can also be frustrated for ferromagnetic interactions with a strong local Ising anisotropy, leading to 'spin ice' behaviour[9]. In general, the degeneracy of the magnetic ground states may be lifted by perturbations arising from chemical disorder or additional magnetic interactions. These include further-neighbour exchange[4], anisotropy[10] and dipolar interactions[11]. Consequently, most antiferromagnetic pyrochlores undergo either spin-glass-like or long-range-ordering transitions[10,12–14]. $Tb_2Ti_2O_7$ is the only one that remains in a fluctuating paramagnetic state down to 70 mK (ref. 8), although spin glass behaviour below 70 mK has been claimed[15]. Muon spin relaxation[8] and neutron scattering[8,16,17] show that the Tb spins begin to develop short-range antiferromagnetic correlations below 100 K.

The single-ion ground state in $Tb_2Ti_2O_7$ is a crystal-field doublet, which interacts with its neighbours via superexchange and dipolar coupling. Given these simple interactions, the absence of magnetic order is surprising[8,16,18]. Further interactions, such as mixing with higher crystal-field states, may therefore play a role in stabilizing the spin liquid state[19]. Applied pressure offers an opportunity to study this stability, by perturbing the balance of the various interactions, which have different dependences on interatomic distance.

Neutron diffraction is the only way to obtain full information about the microscopic spin arrangement. We used Kurchatov-LLB (Laboratoire Léon Brillouin) pressure cells with sapphire anvils, the only apparatus that allows neutron scattering at both very low temperatures (1.4 K) and very high pressures, $P < 10$ GPa (ref. 20). NaCl as the pressure-transmitting medium provides a quasi-hydrostatic pressure, with a non-uniform component estimated to be less than 5%. The pressure was measured by the ruby fluorescence technique with a precision of ±0.1 GPa. The neutron diffraction spectra were recorded on the specialized high-pressure powder

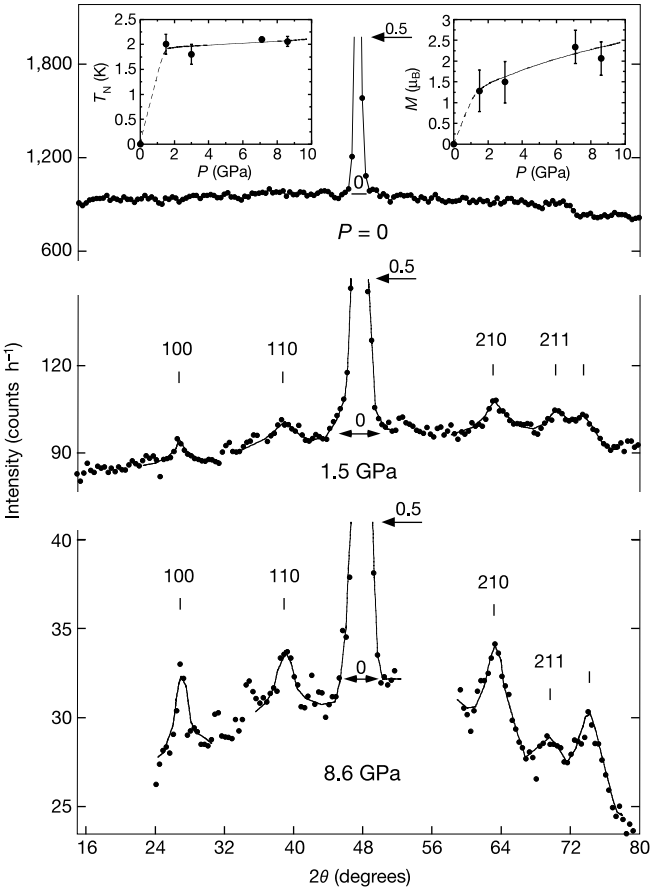

Figure 1 $Tb_2Ti_2O_7$: raw neutron diffraction spectra (neutron counts per hour) for three pressures P at 1.4 K. The incident neutron wavelength is 4.741 Å. Intensity scales are chosen to show the magnetic peaks as compared with the 111 structural peak. Half intensity of the 111 peak is shown at the centre of the spectra. Insets: the Néel temperature, T_N (left), and ordered magnetic moment at 1.4 K, M (right), versus pressure.

